Research Article | Vol. 25, No. 3 | 6 Feb 2017 | OPTICS EXPRESS 1646

Optics EXPRESS

Spatial characterization of Bessel-like beams for strong-field physics

ADAM M. SUMMERS,[1] XIAOMING YU,[2] XINYA WANG,[2] MAXIME RAOUL,[3] JOSH NELSON,[1] DANIEL TODD,[1] STEFAN ZIGO,[1] SHUTING LEI,[2] AND CARLOS A. TRALLERO-HERRERO[1,*]

[1]*J. R. Macdonald Lab., Kansas State University, 116 Cardwell Hall, Manhattan, KS 66506 USA*
[2]*Department of Industrial and Manufacturing Systems Engineering, Kansas State University, Manhattan, KS 66506, USA*
[3]*Ecole Centrale de Marseille, 38 Rue Frederic Joliot Curie, 13013 Marseille, France*
[*]*trallero@phys.ksu.edu*

Abstract: We present a compact, simple design for the generation and tuning of both the spot size and effective focal length of Bessel-like beams. In particular, this setup provides an important tool for the use of Bessel-like beams with high-power, femtosecond laser systems. Using a shallow angle axicon in conjunction with a spherical lens, we show that it is possible to focus Bessel-like modes to comparable focal spot sizes to sharp axicons while maintaining a long effective focal length. The resulting focal profiles are characterized in detail using an accurate high dynamic range imaging technique. Quantitatively, we introduce a metric ($R_{0.8}$) which defines the spot-size containing 80% of the total energy. Our setup overcomes the typical compromise between long working distances and small spot sizes. This is particularly relevant for strong-field physics where most experiments must operate in vacuum.

OCIS codes: (320.0320) Ultrafast optics; (320.5540) Pulse shaping; (110.4155) Multiframe image processing.

References and links

1. S. Akturk, "Tailored-beam ultrashort laser pulses," Quantum Phys. Lett. **112**, 97–112 (2012).
2. D. McGloin and K. Dholakia, "Bessel beams: diffraction in a new light," Contemp. Phys. **46**(1), 15–28 (2005).
3. V. Jarutis, R. Paškauskas, and A. Stabinis, "Focusing of Laguerre-Gaussian beams by axicon," Opt. Commun. **184**(1-4), 105–112 (2000).
4. M. Lei and B. Yao, "Characteristics of beam profile of Gaussian beam passing through an axicon," Opt. Commun. **239**(4-6), 367–372 (2004).
5. R. Grunwald, M. Bock, V. Kebbel, S. Huferath, U. Neumann, G. Steinmeyer, G. Stibenz, J.-L. Néron, and M. Piché, "Ultrashort-pulsed truncated polychromatic Bessel-Gauss beams," Opt. Express **16**(2), 1077–1089 (2008).
6. D. G. Grier, "A revolution in optical manipulation," Nature **424**(6950), 810–816 (2003).
7. J. Arlt, V. Garces-Chavez, W. Sibbett, and K. Dholakia, "Optical micromanipulation using a Bessel light beam," Opt. Commun. **197**(4-6), 239–245 (2001).
8. J. Durnin, J. Miceli, Jr., and J. H. Eberly, "Diffraction-free beams," Phys. Rev. Lett. **58**(15), 1499–1501 (1987).
9. R. M. Herman and T. A. Wiggins, "Production and uses of diffractionless beams," J. Opt. Soc. Am. A **8**(6), 932–942 (1991).
10. Z. Ding, H. Ren, Y. Zhao, J. S. Nelson, and Z. Chen, "High-resolution optical coherence tomography over a large depth range with an axicon lens," Opt. Lett. **27**(4), 243–245 (2002).
11. C. Snoeyink and S. Wereley, "Single-image far-field subdiffraction limit imaging with axicon," Opt. Lett. **38**(5), 625–627 (2013).
12. J. Arlt, K. Dholakia, J. Soneson, and E. M. Wright, "Optical dipole traps and atomic waveguides based on Bessel light beams," Phys. Rev. A **63**(6), 063602 (2001).
13. A. A. Babin, D. V. Kartashov, and D. I. Kulagin, "Focusing femtosecond radiation with an axicon," Quantum Electron. **32**(4), 308–310 (2002).
14. D. N. Schimpf, J. Schulte, W. P. Putnam, and F. X. Kärtner, "Generalizing higher-order Bessel-Gauss beams: analytical description and demonstration," Opt. Express **20**(24), 26852–26867 (2012).
15. P. Saari and H. Sõnajalg, "Pulsed Bessel beams," Laser Phys. **7**, 32–39 (1997).
16. D. Faccio, E. Rubino, A. Lotti, A. Couairon, A. Dubietis, G. Tamošauskas, D. G. Papazoglou, and S. Tzortzakis, "Nonlinear light-matter interaction with femtosecond high-angle Bessel beams," Phys. Rev. A: At. Mol. Opt. Phys. **85**(3), 033829 (2012).
17. P. Polynkin, M. Kolesik, A. Roberts, D. Faccio, P. Di Trapani, and J. Moloney, "Generation of extended plasma channels in air using femtosecond Bessel beams," Opt. Express **16**(20), 15733–15740 (2008).

#280225 http://dx.doi.org/10.1364/OE.25.001646
Journal © 2017 Received 10 Jan 2017; revised 11 Jan 2017; accepted 12 Jan 2017; published 23 Jan 2017

Optics EXPRESS

18. X. Yu, C. A. Trallero-Herrero, and S. Lei, "Materials processing with superposed Bessel beams," Appl. Surf. Sci. **360**, 833–839 (2016).
19. F. Courvoisier, J. Zhang, M. K. Bhuyan, M. Jacquot, and J. M. Dudley, "Applications of femtosecond Bessel beams to laser ablation," Appl. Phys., A Mater. Sci. Process. **112**(1), 29–34 (2013).
20. T. Auguste, O. Gobert, and B. Carré, "Numerical study on high-order harmonic generation by a Bessel-Gauss laser beam," Phys. Rev. A: At. Mol. Opt. Phys. **78**(3), 033411 (2008).
21. C. Altucci, R. Bruzzese, D. D'Antuoni, C. de Lisio, and S. Solimeno, "Harmonic generation in gases by use of Bessel–Gauss laser beams," J. Opt. Soc. Am. B **17**(1), 34 (2000).
22. M. Nisoli, E. Priori, G. Sansone, S. Stagira, G. Cerullo, S. De Silvestri, C. Altucci, R. Bruzzese, C. de Lisio, P. Villoresi, L. Poletto, M. Pascolini, and G. Tondello, "High-brightness high-order harmonic generation by truncated bessel beams in the sub-10-fs regime," Phys. Rev. Lett. **88**(3), 033902 (2002).
23. L. Van Dao, K. B. Dinh, and P. Hannaford, "Generation of extreme ultraviolet radiation with a Bessel-Gaussian beam," Appl. Phys. Lett. **95**(13), 131114 (2009).
24. G. P. Agrawal, *Fiber-Optic Communication Systems,* 4th ed. (Wiley, 2010).
25. X. Tsampoula, V. Garcés-Chávez, M. Comrie, D. J. Stevenson, B. Agate, C. T. A. Brown, F. Gunn-Moore, and K. Dholakia, "Femtosecond cellular transfection using a nondiffracting light beam," Appl. Phys. Lett. **91**(5), 053902 (2007).
26. E. Wolf, *Progress in Optics* (Elsevier, 2009), Vol. 54.
27. M. C. Chen, P. Arpin, T. Popmintchev, M. Gerrity, B. Zhang, M. Seaberg, D. Popmintchev, M. M. Murnane, and H. C. Kapteyn, "Bright, coherent, ultrafast soft X-ray harmonics spanning the water window from a tabletop light source," Phys. Rev. Lett. **105**(17), 173901 (2010).
28. T. Popmintchev, M.-C. Chen, A. Bahabad, M. Gerrity, P. Sidorenko, O. Cohen, I. P. Christov, M. M. Murnane, and H. C. Kapteyn, "Phase matching of high harmonic generation in the soft and hard X-ray regions of the spectrum," Proc. Natl. Acad. Sci. U.S.A. **106**(26), 10516–10521 (2009).
29. M. B. Gaarde, J. L. Tate, and K. J. Schafer, "Macroscopic aspects of attosecond pulse generation," J. Phys. At. Mol. Opt. Phys. **41**(13), 132001 (2008).
30. C. Trallero-Herrero, C. Jin, B. E. Schmidt, A. D. Shiner, J.-C. Kieffer, P. B. Corkum, D. M. Villeneuve, C. D. Lin, F. Légaré, and A. T. Le, "Generation of broad XUV continuous high harmonic spectra and isolated attosecond pulses with intense mid-infrared lasers," J. Phys. At. Mol. Opt. Phys. **45**(1), 011001 (2012).
31. M. B. Gaarde and K. J. Schafer, "Generating single attosecond pulses via spatial filtering," Opt. Lett. **31**(21), 3188–3190 (2006).
32. P. Balcou, P. Salieres, A. L'Huillier, and M. Lewenstein, "Generalized phase-matching conditions for high harmonics: the role of field-gradient forces," Phys. Rev. A **55**(4), 3204–3210 (1997).
33. H. Dachraoui, T. Auguste, A. Helmstedt, P. Bartz, M. Michelswirth, N. Mueller, W. Pfeiffer, P. Salieres, and U. Heinzmann, "Interplay between absorption, dispersion and refraction in high-order harmonic generation," J. Phys. At. Mol. Opt. Phys. **42**(17), 175402 (2009).
34. A. Averchi, D. Faccio, R. Berlasso, M. Kolesik, J. V. Moloney, A. Couairon, and P. Di Trapani, ""Phase matching with pulsed Bessel beams for high-order harmonic generation," Phys. Rev. A: At. Mol. Opt. Phys. **77**(2), 021802 (2008).
35. M. Nisoli, S. De Silvestri, and O. Svelto, "Generation of high energy 10 fs pulses by a new pulse compression technique," Appl. Phys. Lett. **68**(20), 2793–2795 (1996).
36. F. Krausz and M. Ivanov, "Attosecond physics," Rev. Mod. Phys. **81**(1), 163–234 (2009).
37. E. A. J. Marcatili and R. A. Schmeltzer, "Hollow metallic and dielectric waveguides for long distance optical transmission and lasers," Bell Syst. Tech. J. **43**(4), 1783–1809 (1964).
38. M. Nisoli, S. De Silvestri, O. Svelto, R. Szipöcs, K. Ferencz, C. Spielmann, S. Sartania, and F. Krausz, "Compression of high-energy laser pulses below 5 fs," Opt. Lett. **22**(8), 522–524 (1997).
39. P.-A. Bélanger and M. Rioux, "Ring pattern of a lens-axicon doublet illuminated by a Gaussian beam," Appl. Opt. **17**(7), 1080–1088 (1978).
40. V. Belyi, A. Forbes, N. Kazak, N. Khilo, and P. Ropot, "Bessel-like beams with z-dependent cone angles," Opt. Express **18**(3), 1966–1973 (2010).
41. H. Valtna-Lukner, P. Bowlan, M. Lõhmus, P. Piksarv, R. Trebino, and P. Saari, "Measuring the spatio-temporal field of diffracting ultrashort Bessel-type light bullets," Opt. Express **17**, 2 (2009).
42. C. Vinegoni, C. Leon Swisher, P. Fumene Feruglio, R. J. Giedt, D. L. Rousso, S. Stapleton, and R. Weissleder, "Real-time high dynamic range laser scanning microscopy," Nat. Commun. **7**, 11077 (2016).
43. S. Akturk, B. Zhou, B. Pasquiou, M. Franco, and A. Mysyrowicz, "Intensity distribution around the focal regions of real axicons," Opt. Commun. **281**(17), 4240–4244 (2008).
44. F. Gori, C. Guattari, and C. Padovani, "Bessel-Gauss beams," Opt. Commun. **64**(6), 491–495 (1987).
45. O. Brzobohatý, T. Cizmár, and P. Zemánek, "High quality quasi-Bessel beam generated by round-tip axicon," Opt. Express **16**(17), 12688–12700 (2008).
46. J. Dudutis, P. GeČys, and G. RaČiukaitis, "Non-ideal axicon-generated Bessel beam application for intra-volume glass modification," Opt. Express **24**(25), 28433–28443 (2016).
47. C. Xie, V. Jukna, C. Milián, R. Giust, I. Ouadghiri-Idrissi, T. Itina, J. M. Dudley, A. Couairon, and F. Courvoisier, "Tubular filamentation for laser material processing," Sci. Rep. **5**, 8914 (2015).
48. W. C. Wallace, O. Ghafur, C. Khurmi, S. Sainadh U, J. E. Calvert, D. E. Laban, M. G. Pullen, K. Bartschat, A. N. Grum-Grzhimailo, D. Wells, H. M. Quiney, X. M. Tong, I. V. Litvinyuk, R. T. Sang, and D. Kielpinski,

Optics EXPRESS

"Precise and accurate measurements of strong-field photoionization and a transferable laser intensity calibration standard," Phys. Rev. Lett. **117**(5), 053001 (2016).
49. A. D. Shiner, C. Trallero-Herrero, N. Kajumba, H. C. Bandulet, D. Comtois, F. Légaré, M. Giguère, J. C. Kieffer, P. B. Corkum, and D. M. Villeneuve, "Wavelength scaling of high harmonic generation efficiency," Phys. Rev. Lett. **103**(7), 073902 (2009).
50. A. D. Shiner, C. Trallero-Herrero, N. Kajumba, B. E. Schmidt, J. B. Bertrand, K. T. Kim, H.-C. Bandulet, D. Comtois, J.-C. Kieffer, D. M. Rayner, P. B. Corkum, F. Légaré, and D. M. Villeneuve, "High harmonic cutoff energy scaling and laser intensity measurement with a 1.8 μm laser source," J. Mod. Opt. **60**(17), 1458–1465 (2013).
51. S. Zigo, A. T. Le, P. Timilsina, C. T. Herrero, "Ionization study of isomeric molecules in strong-field laser pulses," Sci. Rep. (to appear).

1. Introduction and motivation

Bessel-Gauss beams or Bessel-like beams have a series of enticing and desirable properties over standard Gaussian beams [1,2]. Among the most notable is the ability to overcome limitations of the Rayleigh range [3–5]. Bessel beams maintain focused, on-axis peak intensity for much longer distances than focused Gaussian beams. Bessel beams have been successfully used for numerous applications including optical tweezers [6,7], quasi-diffractionless beam propagation [8,9], optical coherence tomography [10], subdiffraction limit microscopy [11] and particle trapping [12]. Bessel beams are also particularly exciting for uses in ultrafast, strong-field science [1,13–15]. Specific applications include plasma filament generation [16,17], laser machining [18,19], high harmonic generation (HHG) [20–23], optical fiber coupling [24] and optical cellular transfection [25]. In several of these applications Bessel-like beams can offer orders of magnitude improvement over conventional Gaussian beams.

There are several techniques that can be used to generate Bessel-like beams. These include diffractive optics, spatial-light-modulators (SLM's), as well as axicons [26]. The most common way of generating a Bessel beam is with a transmissive axicon. Tranmissive axicons have a number of advantages over other methods, such as simplicity to implement and low energy loss. While SLM's allow for a great degree of control, they can be expensive and complicated to implement. SLM's also have fairly low peak power and average power damage thresholds and thus can only be used with moderate pulse energies and repetition rates. By changing the sharpness or apex angle of the axicon and the properties of the input beam it is possible to tailor the focal profile of the Bessel beam.

Tailoring Bessel beams to strong-field physics has many benefits. For example, in HHG the process of phase matching plays a critical role in the overall conversion efficiency of the fundamental beam into the generated harmonics [27–29]. Phase matching is also extremely important for the generation of isolated attosecond pulses [30,31]. Increasing the length over which a high, on-axis intensity is maintained, has been shown to greatly aid in better phase matching conditions for the generation of higher-order harmonics [32,33]. Thus, Bessel beams produced using axicons can significantly aid in the production of high-flux vacuum ultraviolet (VUV) and extreme ultraviolet (XUV) pulses [23,34]. Additionally, in the far field, beams produced using axicons transform into so called "donut modes" where the on-axis intensity goes to zero. This could prove to be a large benefit in separating the fundamental laser beam from the generated harmonics though the use of a simple aperture that allows the HHG beam to pass while blocking the residual (undesired) fundamental beam.

An additional potential application for intense Bessel beams is the generation of few-cycle laser pulses. Many ultrafast studies use few-cycle pulses produced by broadening the spectral bandwidth of the pulse using self-phase modulation (SPM). The most common way of doing this is to focus the beam into a hollow-core-capillary filled with a noble gas [35,36]. The capillary then guides the focused beam over a long distance (≥1 meter) where the high intensity interaction with the gas results in SPM. Relatively low coupling and transmission efficiencies limit the overall transmission [37,38]. As the waveguide is cylindrical, the eigenmodes for a traveling EM wave are solutions to Bessel's equation [24,37]. Transforming

Optics EXPRESS

the input profile to a Bessel mode could result in an overall increase of the transmission efficiency [24].

However, before high energy Bessel beams can be widely used, several technical challenges need to be overcome. Most notably, as a large number of experiments using ultrafast lasers are performed in vacuum chambers, the laser light needs to be coupled into the system through a window. The fluence on such windows needs to be kept low to avoid damage and undesired nonlinear effects. This is frequently overcome using long focal length, or shallow, optics with the window placed far away from the focus. This is difficult to do using just an axicon as shallow axicons produce a very large "focal waist". This limits the max achievable intensity to prohibitively low values. Sharp angle axicons can produce very tight foci but also have extremely short working distance, unsuitable for coupling into vacuum.

In this study, we present a simple, compact and flexible setup for generating relatively tight focusing Bessel-like beams with long effective working distances. By placing a positive, spherical lens before a shallow angle axicon it is possible to produce tight focal spot sizes while keeping the working distance long enough to allow for high-energy laser pulses to be coupled into vacuum. Additionally, by adjusting the ratio of the spherical lens focal length to the distance between the two optics, a very large array of spot sizes can be produced using a single axicon. It should be mentioned that several published studies exist using a similar setup [23,39–41] but a full beam characterizatin is still lacking, especially for femtosecond pulses. We present detailed characterization measurements for a variety of spherical lens focal lengths and distances between the axicon and focusing lens using both pulsed and continuous-wave lasers. These measurements use a new form of high dynamic range (HDR) imaging to accurately measure the intensity profile of focused Bessel beams over a large scanning range. A somewhat similar HDR approach was recently developed for use in multiphoton fluorescence microscopy [42]. Both the ability to generate tight foci with long effective working distances and the extreme tunability of our setup are promising for using Bessel beams in strong-field science.

2. Optical setup and beam characterization

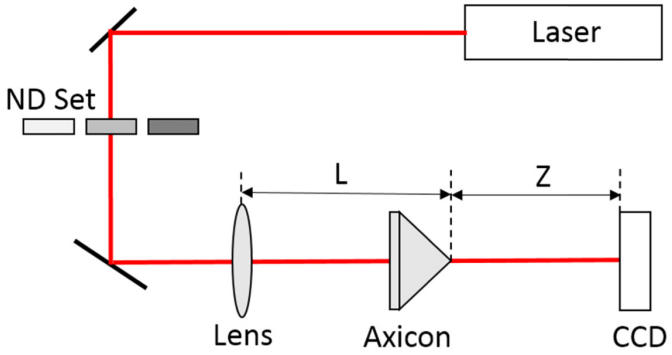

Fig. 1. Experimental setup.

A schematic of the experimental setup is shown in Fig. 1. For comparison purpose, we use two laser sources, a continuous-wave HeNe laser with 633-nm wavelength and a Chirp Pulse Amplification (CPA) based femtosecond laser system delivering 35-fs pulses with a center wavelength of 795 nm, pulse energies of up to 2 mJ, and a repetition rate of 2 kHz. Three neutral density (ND) filters (ND values of 0.1, 1.0 and 2.0, Thorlabs) are used to attenuate the beam to different levels for our high-dynamic-range (HDR) imaging scheme. In order to ensure a high degree of accuracy the ND filters are individually calibrated for each of the laser sources, 632 nm and 795 nm, prior to use in the axicon-lens setup. The measured ND

Optics EXPRESS

values are 0.052, 0.97 and 1.85 for 632 nm, and 0.063, 1.07 and 1.84 for 795 nm. Three positive spherical lenses with focal lengths of 100, 200 and 300 mm are placed in front of the axicon (Edmund Optics), which has a base angle of 1° and diameter of 25.4 mm. The distance (L) between the lens and the axicon is changed in order to tune the focal spot size and the axial depth of field of the Bessel-like beam. A camera (Mightex, SME-B050-U B/W) is used to record beam profiles at various axial (Z) positions (Z = 0 is defined at the axicon tip). For some measurements, a circular piece of aluminum foil of 2-mm in diameter is placed directly in front of the axicon to block the central portion of the laser in order to reduce intensity modulation caused by the blunt axicon tip [43].

One key issue in the focal profile analysis is the accurate determination of intensity distribution. This issue becomes more difficult for analyzing laser beams with large intensity variations. Bessel-like beams are an extreme example of such a case. Due to the fact that each of the outer rings in an ideal Bessel beam contains the same amount of energy [44], the intensity of each ring falls off as a function of radius. Imaging with high bit-depth is desired to capture both the outer rings and the minima in between rings. In this work, we use the technique of high dynamic range imaging to extend the image bit-depth. This process is shown in Fig. 2. At each axial (Z) position, three distinct images (Figs. 2(a)-2(c)) are captured, each using a separate ND filter. Due to the limited, 8-bit depth of the camera, either high intensity regions are saturated (Figs. 2(b) and 2(c)), or low intensity regions are not visible (Fig. 2(a)). The HDR image is generated algorithmically by replacing saturated pixels of the middle image (ND2) with the corresponding, unsaturated, pixels in the highly attenuated image (ND1). Similarly, pixels with a low value in the middle image are replaced with the corresponding pixels in the least attenuated image (ND3). Before combination, the raw pixel values of all images are multiplied by the corresponding optical density values. The result is a combined image where both high and low intensity regions are present, as shown in Fig. 2(d). The low-intensity, outer rings are emphasized in Fig. 2(e) by plotting the square root of the intensity.

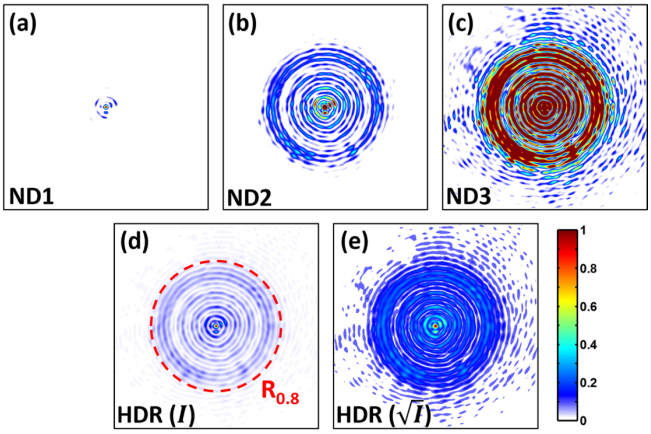

Fig. 2. An example showing HDR image processing. Images (a)-(c) are obtained using three ND filters with the femtosecond laser. Combined high dynamic range (HDR) images are shown in (d) with linear intensity (*I*) and in (e) with square root *I*. 80% of the total energy falls within the red circle in (d) with a radius of $R_{0.8}$.

This technique can significantly increase effective bit depth of the camera. As such, detailed and accurate measurements can be performed without the need for prohibitively expensive, high bit depth cameras. The effective bit-depth of the combined images is approximately 14-bits, representing a 64-fold increase in detection range over a single 8-bit image.

Optics EXPRESS

The intensity of focused Bessel-like beams does not decrease monotonically as a function of radial distance away from the center beam. This makes a quantitative study of the focal properties of Bessel-like beams challenging. Standard parameters such as the full-width-at-half-maximum (FWHM) and $1/e^2$ beam waist do not accurately describe the focal profile. For this study, we use a more suitable parameter, the radius at which 80% of the beam energy falls within, $R_{0.8}$. Shown as the dotted red line in Fig. 2(d), this parameter captures the most usable part of the mode.

3. Results and discussion

We examine the profiles of Bessel-like beams generated with the combination of a lens and an axicon. We use two laser sources, a continuous-wave (CW) HeNe laser and a femtosecond laser (Kansas Light Source) delivering 35 fs FWHM pulses. Figure 3 shows the beam shape on the transverse plane (Figs. 3(a) and 3(b)) and the longitudinal sections (Figs. 3(c) and 3(d)), for the two laser types. These measurements were taken using a lens with a focal length of 200 mm and a distance L of 10 mm.

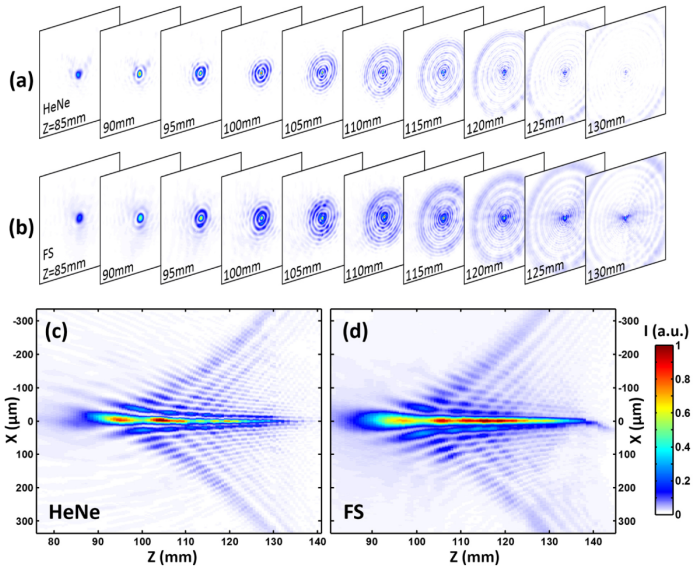

Fig. 3. (a, b) Bessel-like beams observed at various distances (Z) from the axicon for (a) HeNe and (b) femtosecond (FS) lasers. (c, d) Longitudinal profiles of laser beams for (c) HeNe and (d) femtosecond lasers. Intensities are normalized to the peak values in the two cases.

We observe similarities between the two cases. Bright cores start to form at around Z = 85 mm, where Z is the distance between the axicon and the observation plane. Concentric rings appear at a further distance (Z = 90-100 mm), resembling those of Bessel and Bessel-Gauss beams [8,44]. However, a few key differences are observed compared to the ideal Bessel and Bessel-Gauss beams. We attribute most these differences to the imperfect axicon tip. First, as L changes, the central cores vary in intensity, which is more noticeable on the longitudinal profiles (Figs. 3(c) and 3(d)). This has been linked in previous work [43] to an imperfect axicon tip. We show later that such oscillations can be partially suppressed by blocking the central part of the input beam.

The most striking and important feature observed in these measurements is the incredibly long distance over which the peak intensity is maintained. This is most apparent for the pulsed laser. The central core intensity stays at or above 50% of the peak intensity for over 40 mm, more than 20 times longer than a Gaussian beam with a similar focal diameter. The peak intensity occurs at approximately 105 mm, much longer than if just a sharp angle axicon was

Optics EXPRESS

used individually. The combination of both optics allow for both long depth of field and long working distance simultaneously.

Second, we observe reduced intensity for the inner rings at Z>100 mm. For instance, on the Z = 110 mm images in Figs. 3(a) and 3(b), one can see that some inner rings have lower intensity (in whiter color) compared to the outer rings. This intensity modulation is more apparent in Figs. 3(c) and 3(d), where one can see discrete, symmetric structures around the cores at Z>100 mm.

We also observe differences between the HeNe and pulsed laser. The HeNe beam shape is smaller than the pulsed beam, in both transverse and axial dimension. This is due to the fact the HeNe wavelength (633 nm) and input beam size (7.4 mm, $1/e^2$ size) are both smaller than those of the pulsed laser (790 nm and 9.8 mm, respectively). We point out that even though the input beam diameters are different for the two lasers, the features observed in Fig. 3 are present for other beam size because of simple linear relationship between input beam size and dimension of resultant Bessel-like beam [43]. One difference of particular interest is the reduced fidelity of outer rings for the pulsed laser, which is more noticeable by comparing Fig. 3(d) with Fig. 3(c). As has been pointed out by others [40,44], the temporal aspect of the pulsed laser can alter the spatial aspect. The difference is due to the bandwidth content in a femtosecond pulse compared to CW lasers [5]. This is an important effect to keep in mind when generating Bessel-like beams with pulsed lasers. However, it has also been shown that the center mode is not as affected by space-time-coupling effects as the outer rings [45]. Many of the applications of Bessel-like beams seek to use just the central portion of the mode. From these cases the bandwidth effects on the spatial distribution should be negligible.

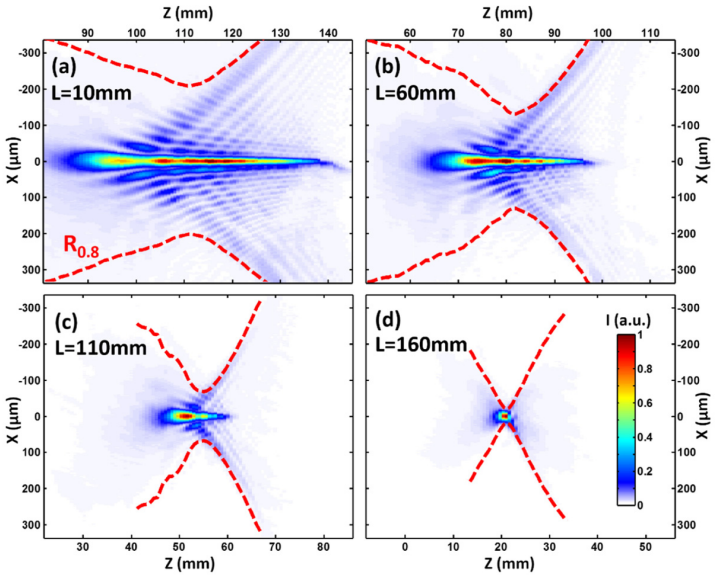

Fig. 4. Longitudinal sections of femtosecond Bessel-like beams generated at various lens-axicon distances (L). The focal length of the lens is 200 mm. Red dashed lines mark the boundary of 80%-energy beam size ($R_{0.8}$).

The pulse duration of the Bessel-like beam was not measured in this study. However, it is not expected to significantly differ from pulse durations achievable using a standard transmissive lens [41]. We believe this is particularly so for the case of a shallow axicon like the one used in this study. When using a CPA based laser any added Group velocity dispersion (GVD) due to the axicon thickness can be compensated for in the final compression state of the laser. However, as with any transmissive setup, compensation for

Optics EXPRESS

GVD becomes more difficult when using few-cycle pulses. In this case it would be preferable, albeit more difficult, to use a purely reflective version of our setup.

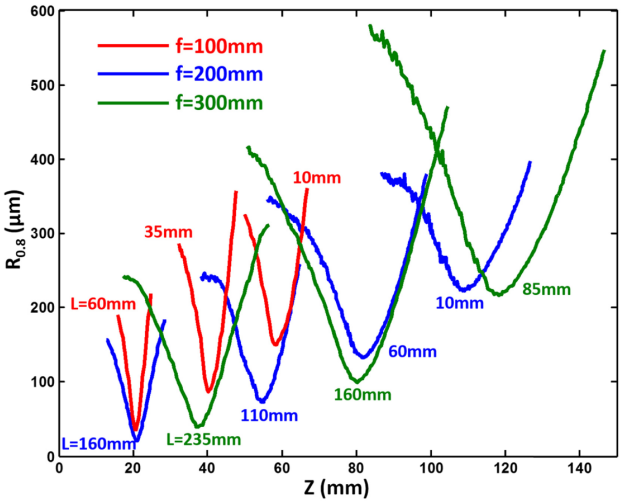

Fig. 5. The 80%-energy beam size measured for three focal lengths (f) and various distances from the axicon (L). Axicon is at Z = 0.

Next, we investigate the beam profiles for various lens-to-axicon distance L. The results are shown in Fig. 4 for L = 10, 60, 110 and 160 mm. The focal length of the lens is f = 200 mm. We can see that as L increases, the depth of field decreases along with the focal spot size. This is expected. As L is increased, the axicon position moves closer to the focal point of the spherical lens. The axicon is a positive (focusing) element so when placed between the lens and its focal point the axicon further reduces the total focal length. This of course results in a shortened depth of field for the system as a whole. Even though the axial length is reduced, the beam shape maintains similar characteristics, e.g., bright cores and modulated ring structures, between L = 10 mm to L = 110 mm. At L = 160 mm, for which the axicon is placed close to the focal plane of the lens (f = 200 mm), the ring structures disappear, showcasing the asymptotic case when L approaches f. This, again, is attributed to the blunt axicon tip combined with the reduced beamsize incident on the axicon. These figures illustrate the large degree of tunability achievable through changing the distance between the lens and axicon. It is possible to change the 80% minimum spot size by over a factor of two through this simple parameter.

Figure 5 demonstrates the flexibility of tuning axial length of the generated Bessel-like beams by changing the lens-axicon distance L and the focal length of the lens. To this end, we choose three focal lengths, f = 100, 200 and 300 mm, and record beam profile for various L distances. Figure 5 shows the 80% energy radii $R_{0.8}$ calculated for each data set. We can see that for each focal length, the $R_{0.8}$ curves move closer to the axicon when L increases. The minima of the curves point to the Z-position where laser energy is most concentrated, and their values are the corresponding smallest spot size of 80% total energy. While the three sets of curves from three focal lengths have similar shape, longer focal lengths lead to a longer axial extent and thus wider curves. This can be seen by comparing f = 200 mm, L = 160 mm and f = 300 mm, L = 160 mm curves with the f = 100 mm, L = 60 mm and f = 200 mm, L = 60 mm curves, respectively. These results again highlight the overall tunability of our optical setup. There exists a trade-off between the location of the beam and the beam spot size, as with any optical system. With the same lens focal length, moving the beam further away from the axicon (smaller L) causes a larger spot size, and vice versa. It of course remains important to keep the fluence of the beam incident on the axicon low enough to avoid damage and

Optics EXPRESS

nonlinear effects in the glass. As such, it may not be possible to use all of the parameter space shown in Fig. 5 when using extremely high peak power sources.

The on-axis intensity variation has been attributed to an imperfect axicon tip, which adds interference to the properly refracted outer beam [45,46]. The modulation can be partially suppressed by blocking the central part of the beam [43] or by spatial filtering [45]. To demonstrate that this method also applies to a femtosecond laser, we cut a circular piece of aluminum foil with 2-mm diameter and attach it to a glass microscope slide. We then placed the assembly before the lens so that the foil blocks the central portion of the beam. All other optics are unaltered. The Bessel-like beam generated in this way is shown in Fig. 6(b) in comparison with the original beam (Fig. 6(a)). Red curves are the on-axis intensity averaged around X = 0 with a width of 30 μm. This width is approximately the size of the beam core. The partial suppression of intensity variation (as compared to Fig. 6(a)) can be seen, especially in the front part (L<110 mm) of the beam. Besides, the modulation in the rings, while not completely removed, is also suppressed.

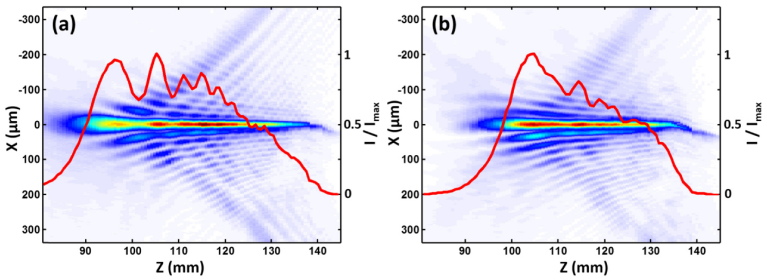

Fig. 6. Beam profiles for (a) original and (b) center-blocked input beam. Red curves are intensity profiles averaged around the cores (X = 0, average width 30 μm) normalized to the maximum intensity. f = 200 mm, L = 10 mm.

The red lineouts shown in Fig. 6 have been normalized to the maximum intensity. For 1mJ pulse energies, with a temporal width of 35 fs, our setup will produce peak intensities of approximately 5×10^{14} W/cm^2, calculated using the relations between energy, and pulse duration. One should also note that while we have use the setup with mJ of energy per pulse, the laser power/energy used in this study is low (< 1 mW for the HeNe laser and <1 μJ for the femtosecond laser). Such low energies are necessary to avoid any nonlinear effect such as plasma generation in air [47] and to prevent damage to the camera sensor.

Since many strong-field studies, such as high harmonic generation, are conducted in vacuum, our results can provide adequate assessment of beam profiles when used for those experiments. As pointed out in [44] a theoretical description of the spatial properties of an axicon is possible, however it is extremely sensitive to deformations of the axicon tip. While our setup can compensate for the position and size of the focus by tuning the lens-axicon distance, the sensitivity to the axicon shape does posses a challenge for an *a priori* determination of the peak intensity. We would like to point out that an accurate measurement of the peak intensity is extremely hard for intense femtosecond pulses and it still an active area of research [48]. Therefore, we believe that practically it is best to use strong field ionization and a fit to a model for the proper characterization of the peak intensity [49–51].

4. Conclusion

In this work we have characterized the beam profile of a lens-axicon system. We do this characterization for a CW laser and a femtosecond laser. Our observations show that the working distance and spot sizes of Bessel-like beams can be greatly tuned by simply changing the distance of the lens to the axicon. Furthermore, the laser-axicon combination generates beams for which the central core intensity stays at or above 50% of the peak intensity for over 40mm. This “effective Rayleigh range” is more than 20 times longer than a Gaussian beam

Optics EXPRESS

with a similar focal diameter. We show that by changing the lens focal length we can change the working distance greatly, while still keeping small spot sizes. Our measurements are very encouraging for the application of Bessel beams for strong field studies

Funding

U.S. Department of Energy (DOE), Office of Basic Energy Sciences, Chemical Sciences, Geosciences, and Biosciences Division, (DE-FG02-86ER13491); Department of Defense (DoD) through the National Defense Science & Engineering Graduate Fellowship (NDSEG), National Science Foundation (NSF) (CMMI-1537846); National Science Foundation (NSF) (PHYS-1461251)

Acknowledgment

Program Support for CAT-H and SZ was provided through Chemical Sciences, Geosciences, and Biosciences Division, Office of Basic Energy Sciences, U.S. Department of Energy, AMS was supported by the Department of Defense (DoD) through the National Defense Science & Engineering Graduate Fellowship; XY, XW and SL were funded through the National Science Foundation. JN and DT were partially supported through National Science Foundation Research Experience for Undergraduates (REU)